Modeling and simulation of nanowire based field-effect biosensors

Stefan Baumgartner[1], Martin Vasicek[1,2], and
Clemens Heitzinger[1,2,3]

[1] Department of Mathematics, University of Vienna, Austria.
[2] Wolfgang Pauli Institute c/o Department of Mathematics,
University of Vienna, Austria.
[3] Department of Applied Mathematics and Theoretical Physics (DAMTP),
University of Cambridge, UK.

Contents

1 Introduction

The digital revolution was initiated by the invention of the field-effect transistor (FET), for which Shockley, Bardeen, and Brattain were jointly awarded the 1956 Nobel Prize in Physics. Semiconductor transistors and microchips have deeply influenced human society. Also the invention of the first biosensor for blood analysis, invented by Clark and Lyons more than thirty years later, had a life changing effect (Clark and Lyons, 1962). Another eight years later, these two technologies were merged as Bergveld introduced the ion-sensitive field-effect transistor (ISFET). This marks the beginning of sensing technologies based on field-effect transistors (Bergveld, 1970; Schöning and Poghossian, 2006). Beside the use of field-effect transistors as pH sensors, which were also established in 1971 by Matsuo et al. (Janata, 2004), they can be used as versatile tools for the detection of, e.g., ion concentrations, enzymatic reactions, cellular metabolism, and action potentials of living cells (Poghossian et al., 2007).

Since then, biosensor technologies flourished and are of paramount interest (Stern et al., 2010; Tian et al., 2010; Timko et al., 2010). The transducers used in field-effect sensors have changed in recent years due the rise of nanotechnology in medical and biotechnological applications (Patolsky et al., 2006c,a; Stern et al., 2008). Nowadays, the most promising sensing devices are based on nanowires and carbon nanotubes because of their high sensitivity, fast response, and direct electrical readout (Patolsky et al., 2006b). Still, questions of characterization, uniformity and manufacturability need to be addressed before nanoscale biosensors can be mass-produced and used in daily life.

In this review, we discuss the state of the art of the quantitative understanding of the sensing mechanism in nanowire-based field-effect biosensors. Quantitative understanding and predictive simulations allow for the rational design and the optimization of the nanowire sensors.

In the case of carbon-nanotube sensors, it has been reported that the adsorption of biomolecules, e.g., proteins, on a SWNT (single-walled carbon nanotube) results in a sufficient change of conductance (Chen et al., 2003, 2004) for detection due to the field effect. Nonetheless, some problems must be overcome before SWNTs can be used commercially as sensors. For example, the non-specific binding of molecules to the SWNT must be avoided due to the possible change of the dielectric constant of the electric double layer in the aqueous solution, which would cause an unwanted sensor response (Chen et al., 2004).

In recent years, much research on silicon nanowire based sensors has been conducted (Cui et al., 2000, 2001, 2003; Hahm and Lieber, 2004; Patolsky and Lieber, 2005; Wang et al., 2005; Zheng et al., 2005; Li et al., 2006; Patolsky et al., 2007; Stern et al., 2007b,a; Elfström et al., 2008; Gao et al., 2010; Zheng et al., 2010), and high sensitivity and selectivity have been demonstrated.
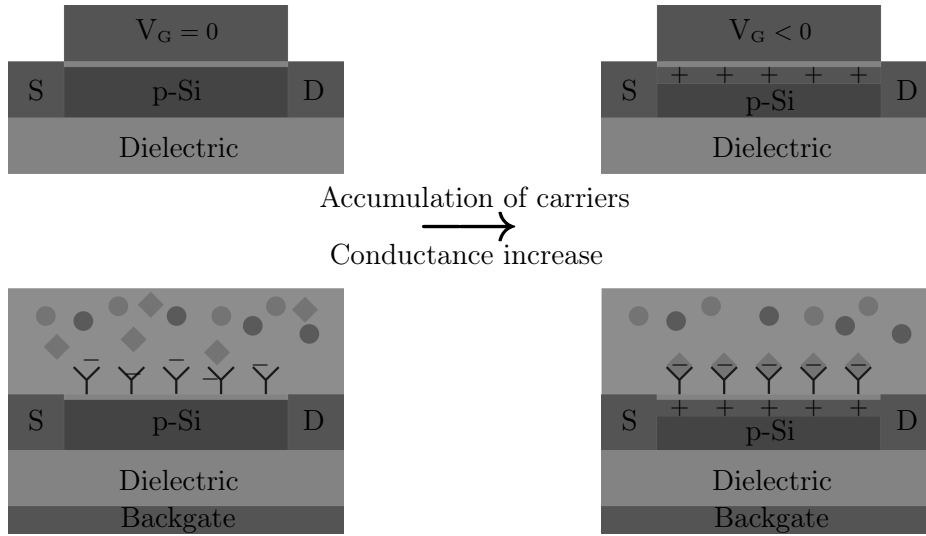
Figure 1: Working principle of a conventional FET (top) and a nanowire field-effect sensor (bottom). In both cases, negative charge at the gate contact or at the nanowire surface leads to an increase of conductance due to accumulation of charge carriers in the semiconductor near the negative charges.

Both DNA and antigen sensors are selective due to the inherent selectivity of DNA-DNA and antibody-antigen binding that is responsible for biological functioning as well.

Physically sound models aid in gaining a deeper insight into the functioning of field-effect sensors. Before we review the models, we summarize the working principle of nanowire field-effect sensors in order to identify the crucial parts for modeling. A p-doped silicon nanowire together with two contacts, a source and a drain contact, is shown in Fig. 1. The nanowire transducer is usually located on top of a dielectric material and covered by a second dielectric material, which is exposed to the ionic solution. A conventional FET structure is also shown in Fig. 1: In this device, a gate contact is located on the top of the dielectric and a negative gate voltage V_G induces an accumulation of positive charge carriers near the silicon surface, which in turn induces an increase of conductance, while a positive gate voltage decreases the conductance.

In field-effect biosensors, the gate contact is replaced by a functionalized boundary layer and an ionic solution containing target molecules. The transducer is functionalized with receptor molecules: in the case of a DNA sensors, the receptors are complementary single-stranded DNA; in the case of antigen sensors, the receptors are the corresponding antibodies. As target molecules in the liquid bind to the receptors, their presence and their partial charges change the charge concentration in the boundary layer, which in

turn modulates the conductance of the nanowire transducer. In Fig. 1, the target molecules carry negative charges and act as a negative gate voltage. Hence accumulation of charge carriers again increases the conductance.

Additional control of the nanowire can be provided by the implementation of a backgate contact, and it plays an important role for the sensitivity of such sensors. Furthermore, it is well-known that the nanowire surface is charged when in contact with water due to chemical reactions, and the surface charge depends on the material and the pH value. Therefore a double layer of ions forms at the surface.

The sensor signal is the measured current through the nanowire, which is modulated due to the gate effect as target molecules bind. In order to calculate the sensor response, it is therefore crucial to consider the boundary layer and the screening of the partial charges of the biomolecules by free ions. The charged boundary layer acts as the gate contact, so that electron and hole transport in the semiconductor must be calculated as a function of the boundary layer, the applied voltages, the geometry of the nanowire, and so forth.

These considerations imply that physically sound modeling and simulation must include firstly the charge concentration in the biofunctionalized boundary layer that gives rise to the field effect and secondly the charge transport in the semiconducting transducer that translates the difference in charge in the boundary layer to the electrical signal. Clearly, the modeling and simulation of field-effect sensors is more complicated than the simulation of conventional FETs due to the additional boundary layer. In the best case, the sensor model is self-consistent meaning that the influences of all charges onto all charges are taken into account while including all applied potentials; this is usually achieved by solving the Poisson equation.

In summary, field-effect biosensors consist of two parts – namely the biofunctionalized boundary layer and the nanowire transducer – that shall be considered self-consistently. Models for the boundary layer, i.e., screening models, are discussed in Section 3. The sensor signal is measured as the current (or change in current) through the nanowire and cannot be explained by the surface models alone; hence suitable charge-transport models are discussed in Section 4. In order to glue these two parts together and solve the multiscale problem inherent in these sensors, a homogenization method is advantageous, which is presented in the following Section 2.

2   Homogenization

As mentioned above, the characteristic length scale of the biomolecules in the boundary layer is smaller than the dimensions of the nanowire by a some orders of magnitude. Problems of this type are called multiscale problems (Pavliotis and Stuart, 2007). A main motivation to study them is the fact

that problems with a microscopic structure are extremely time consuming to solve numerically, since the microscopic structure must be resolved by the numerical grid. Homogenization generally yields equations of similar type, but with homogenized coefficients so that the numerical grids do not have to resolve the microscopic structure anymore. Then previously computationally intractable problems can be solved numerically with reasonable effort.

To obtain the sensor response in terms of the nanowire current, the electrical potential V must be computed everywhere in the simulation domain. Therefore, we consider the Poisson equation

$$-\nabla \cdot (\varepsilon(x,y,z)\nabla V(x,y,z)) = \rho(x,y,z) \qquad \text{in } \Omega, \qquad \text{(1a)}$$

$$V(0+,y,z) = V(0-,y,z) \qquad \text{on } \Gamma, \qquad \text{(1b)}$$

$$\varepsilon(0+,y,z)\partial_x V(0+,y,z) = \varepsilon(0-,y,z)\partial_x V(0-,y,z) \quad \text{on } \Gamma \qquad \text{(1c)}$$

as the basic equation for the electrostatic potential, where V is the electrostatic potential and ε is the permittivity. Furthermore, ρ is the charge concentration in the different materials and will depend on the electrostatic potential itself in the drift-diffusion-Poisson system in Section 4. In the liquid, ρ describes the charge concentration in the ionic solution and also in the boundary layer. The simulation domain Ω is split by the interface Γ into two subdomains. For notational simplicity, the interface is located at $x = 0$. The conditions (1b) and (1c) ensure the continuity of the electric potential and dielectric displacement in the presence of the discontinuity in the permittivity ε at the material boundaries.

The aim of the homogenization method (Heitzinger et al., 2010b) is to replace the Poisson equation and the fast varying charge concentration ρ in the boundary layer by a simpler problem that does not exhibit a microscopic structure and oscillations. Indeed it is found that the complicated, oscillating three-dimensional structure of the biomolecules, their partial charges and screening ions can be replaced by two interface conditions involving only two integral values of the charges in the boundary layer after the cell size in the boundary layer goes to zero.

After homogenization, the original problem (1) becomes the homogenized problem

$$-\nabla \cdot (\varepsilon(x,y,z)\nabla V(x,y,z)) = \begin{cases} \rho(x,y,z) & \text{in } \Omega_{\text{Si}} \cup \Omega_{\text{ox}}, \\ 0 & \text{in } \Omega_{\text{liq}}, \end{cases} \qquad \text{(2a)}$$

$$V(0+,y,z) - V(0-,y,z) = \frac{\zeta(y,z)}{\varepsilon(0+,y,z)} \qquad \text{on } \Gamma, \quad \text{(2b)}$$

$$\varepsilon(0+,y,z)\partial_x V(0+,y,z) - \varepsilon(0-,y,z)\partial_x V(0-,y,z) = -\gamma(y,z) \quad \text{on } \Gamma, \quad \text{(2c)}$$

where V is now the homogenized potential. Here 0+ denotes the limit at the interface Γ on the side of the liquid, while 0− is the limit on the side of the transducer. The fast varying charge concentration in the surface layer is

now, as stated before, subsumed in the macroscopic dipole-moment density ζ and the macroscopic surface-charge density γ of the boundary layer which are defined as

$$\gamma = \int \chi(x, y, z) \mathrm{d}xyz, \tag{3a}$$

$$\zeta = \int x\chi(x, y, z) \mathrm{d}xyz, \tag{3b}$$

where χ is the charge concentration of a cell in the boundary layer.

Both ζ and γ may depend on y and z, the coordinates parallel to the surface, to allow for slow variations of the boundary layer along the interface.

The two interface conditions have the following interpretation: the condition (2b) is a jump in the electrostatic potential and given by the dipole-moment density of the boundary layer, whereas condition (2c) is a jump in the electrostatic field (or more precisely, in the electrostatic displacement) and given by the surface-charge density.

The values of ζ and γ are immediately obtained from the charge concentration in a cell of the boundary layer and can be obtained from any of the boundary-layer models in Section 3.

In summary, the homogenization result decouples the microscopic and macroscopic length scales via the two interface conditions in (2). Details on the efficient implementation of the interface conditions can be found in (Baumgartner and Heitzinger, 2012).

3 The biofunctionalized boundary layer

The biofunctionalized boundary layer is the part of the sensor that provides selectivity. It also translates the presence of biomolecules into a change in the electrostatic potential in the semiconducting transducer due to a redistribution of charge in the boundary layer, when target molecules are present and bound to receptors. Since the sensing concept is based on the field effect, the charge concentration in the boundary layer is crucial for the quantitative understanding of the sensing mechanism.

An accurate model for the boundary layer has to incorporate several effects. In the simplest case, a non-functionalized nanowire is exposed to an electrolyte. Here the charge of the dielectric, e.g., SiO_2 or Si_3N_4, which covers the transducer, depends on the pH value of the electrolyte due to reactions of the electrolyte with hydroxyl groups at the dielectric surface. This is a well-known effect for ISFETs and can be modeled by the site-dissociation model (Bergveld and Sibbald, 1988; Schöning and Poghossian, 2002; Xu et al., 2005) discussed in Section 3.1. This model together with the homogenization result in Section 2 and a charge-transport model for the nanowire can be used for the simulation of pH sensors.

Due to the surface charge of the dielectric, an electric double layer of free ions forms on the transducer. This is a well-known effect that is commonly simulated using Metropolis-Monte-Carlo simulations (Allen and Tildesley, 1987) in order to take into account the finite size of the ions. In addition to the electric double layer, receptor and target molecules with their partial charges are present at the surface, together with a cloud of screening, free ions. Furthermore, the charge state of biomolecules depends on the pH value and the biomolecules and their screening charges interact with the electric double layer.

These questions are – despite recent progress – still an area of active research (Alexov et al., 2011). Hence we describe the three main types of models for these effects in the following: the atomistic approach, i.e., Monte-Carlo simulations, the continuum approach, i.e., the Poisson-Boltzmann equation, and the empirical PROPKA model (Li et al., 2005) are discussed. Compact screening models, such as (Sørensen et al., 2007) have also been developed for the simulation of nanowire sensors (De Vico et al., 2010, 2011).

3.1 The site-dissociation model

The surface of dielectric materials such as SiO_2, Si_3N_4, Al_2O_3, and Ta_2O_5 is charged when in contact with an electrolyte and it is neutral only at the isoelectric point, a specific pH value. This surface charge provides an important baseline value, also regarding the operating regime of the sensor. Since the surface charge is a function of pH value, it was already investigated in ISFET theory. In the following, we give an overview on the site-dissociation model from Bergveld (Bergveld and Sibbald, 1988).

The site-dissociation model assumes that there is an interaction of the electrolyte with discrete surface sites which are amphoteric, i.e., the surface sites can be neutral, a proton donor, or a proton acceptor.

The reactions of the hydroxyl groups (AOH groups, where A is, for example, Si or Al in the case of an SiO_2 or Al_2O_3 surface) at the surface with the H^+ ions in their vicinity relate the equilibrium potential ψ_0 and the H^+ ions. These reactions are expressed in the equilibrium equations

$$AOH \rightleftharpoons^{K_a} AO^- + H_s^+, \tag{4a}$$

$$AOH + H_s^+ \rightleftharpoons^{K_b} AOH_2^+, \tag{4b}$$
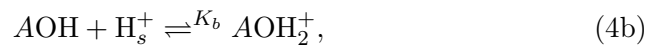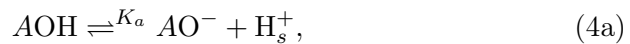
where the dissociation constants K_a and K_b are

$$K_a = \frac{[AO^-][H^+]_s}{[AOH]}, \qquad K_b = \frac{[AOH_2^+]}{[AOH][H^+]_s}$$

and where AO^-, AOH_2^+ and AOH represent the negative (deprotonated), positive (protonated), and neutral surface sites respectively and [.] denotes site concentration.

Furthermore, the concentration of the H$^+$ ions at the surface is related to the bulk concentration via Boltzmann statistics by

$$[\text{H}^+]_s = [\text{H}^+]_b \exp\bigl(-q\psi_0/(kT)\bigr), \tag{5}$$

where q is the elementary charge, k is the Boltzmann constant, and T is the temperature. Using the net surface charge

$$\sigma_0 := q([AOH_2^+] - [AO^-]) \tag{6}$$

and the total number of surface sites per unit area

$$N_s := [AOH] + [AOH_2^+] + [AO^-] \tag{7}$$

together with (3.1) and the assumption that $2(K_a K_b)^{1/2} \ll 1$ yields the equation (see also (Bousse et al., 1983))

$$\ln[\text{H}^+] - \ln(K_a/K_b)^{1/2} = \frac{q\psi_0}{kT} + \sinh^{-1}\left(\frac{\sigma_0}{2qN_s(K_a K_b)^{1/2}}\right) - \ln\left(1 - \frac{\sigma_0}{qN_s}\right). \tag{8}$$

From this equation and the assumption that $\sigma_0 \ll qN_s$, we obtain the relation between the isoelectric point pI (i.e., the pH value where the surface is charge neutral) and the surface potential ψ_0 as the equation

$$2.303(\text{pI} - \text{pH}) = \frac{q\psi_0}{kT} + \sinh^{-1}\left(\frac{q\psi_0}{kT\beta}\right) \tag{9}$$

with

$$\beta := \frac{2q^2 N_s (K_a K_b)^{1/2}}{kTC_L}, \tag{10}$$

where C_L is the constant capacitance of the double layer, i.e., C_L gives the relation $\sigma_0 = \psi_0 C_L$ between σ_0 and ψ_0. Values reported in the literature are $N_s = 5 \cdot 10^{14}\text{cm}^{-2}$ and $C_L = 20\mu\text{Fcm}^{-2}$ for SiO$_2$ (Bergveld and Sibbald, 1988). In the case of an SiO$_2$ surface, the values of β and pI are $\beta = 0.14$ and pI $= 2.2$ (Bergveld and Sibbald, 1988). Finally, the net surface charge can be obtained from the equilibrium potential by multiplication by C_L. For a more detailed description see (Bousse et al., 1983; Harame et al., 1987).

3.2 Screening and biomolecules

The modeling of the electrostatics of biomolecules such as proteins and DNA is not only essential for the simulation of nanowire field-effect sensors, but it is its own important research area. Hence it is not surprising that many approaches of different kinds have been developed, but it is astonishing that none of the methods is significantly better than the rest, each having its own advantages and disadvantages (Lu et al., 2008; Kukic and Nielsen, 2010; Alexov et al., 2011).
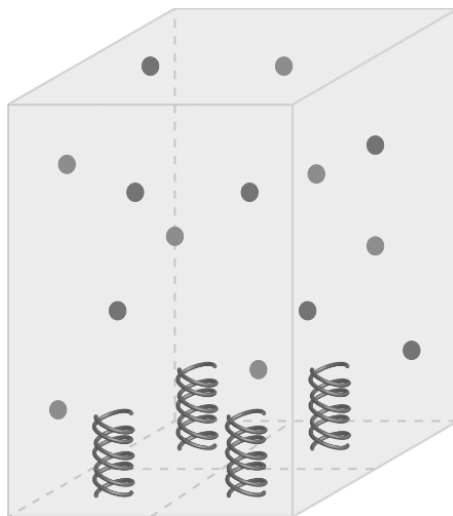
Figure 2: The simulation domain of a constant-voltage Metropolis-Monte-Carlo simulation. Here it contains 2×2 biomolecules at the bottom of the cell. The molecules can be rotated with respect to the surface (Bulyha and Heitzinger, 2011).

In the following, the three main types of biomolecule models are presented. Firstly, a Monte-Carlo algorithm for charged biomolecules at charged surfaces is discussed (Bulyha and Heitzinger, 2011). It is the first of its kind to include charged biomolecules and has been used for sensor simulation (Baumgartner et al., 2011a). The main advantage of the Monte-Carlo approach is that it takes into account the finite size of the ions. Secondly, continuum models are based on the Poisson-Boltzmann equation (PBE), a three-dimensional partial differential equation and one of the main equations in computational chemistry. Thirdly, empirical models have been developed and we give an overview on the PROPKA algorithm, which is one of the most used (Li et al., 2005), also for biosensor simulations (De Vico et al., 2010, 2011).

3.2.1 The Metropolis-Monte-Carlo method

Recently, a Metropolis-Monte-Carlo (MMC) algorithm was developed for the simulation of biomolecules and free ions in the constant-voltage ensemble (Bulyha and Heitzinger, 2011). Here we give an overview on the method and use it for simulations in Section 4.2.

The simulation box is shown in Fig. 2. The biomolecules such as PNA (peptide nucleic acid), single-stranded DNA (ssDNA), or double-stranded DNA (dsDNA), are fixed at the bottom of the box. The length of the oligomers and their linkers can be adjusted to the desired length. The DNA and PNA

oligomers are modeled as cylinders, where the partial charges of the phosphate groups of the backbone are situated on the cylinder surface on a helix while the free ions are excluded. The points where the linkers are attached to the bottom of the box are arranged in an equidistant grid.

The reason for including many biomolecules in a single simulation box is computational. In order to be able to simulate electrolytes with realistic, low ionic concentrations and realistic concentrations of immobilized biomolecules, the simulation domain is quite small compared to the number of free ions; the small number of ions in the box leads to bad statistics in the Monte-Carlo simulation. Hence a larger simulation domain with a grid of molecules provides a sufficient number of ions and leads to much improved statistics.

Each oligomer is bound to the surface by a linker and the biomolecules together with their linkers are simulated as impenetrable cylinders with two hemispheres of the same radius on the top and at the bottom. In the case of PNA oligomers, the cylinders are uncharged, and in the case of ssDNA and dsDNA oligomers, they carry the charges of the phosphate groups of the backbone on their outside. The sizes correspond to the B-DNA conformation of DNA. The oligomers can additionally be rotated with respect to the surface.

The electrolyte in the simulation box is usually Na^+Cl^-. The ions are modeled as charged hard spheres and water is modeled as a continuous medium without structure.

The top and the bottom of the simulation box are impenetrable walls with given charge densities to that the electric field can be controlled. The bottom of the box carries the surface charge as calculated from the site-dissociation model in Section 3.1.

In order to calculate the ion concentration profile, a 3d MMC method must be used in the constant-voltage ensemble because of the voltage drop across the simulation box in sensor application. The constant-voltage ensemble (Kiyohara and Asaka, 2007) can be considered as an extension of the grand-canonical ensemble.

A simulation in the MMC constant-voltage ensemble starts with a random state of the system, i.e., the locations of all ions are random. A new state of the system is generated by randomly adding or deleting a pair of ions, changing the position of an ion while avoiding overlaps, and by transferring a random amount of charge between the walls. Then the potential energy is calculated for each state of the system. The interactions between all pairs of charge types, i.e., the ion-ion, the ion-biomolecule, the ion-plate, the biomolecule-plate, and the plate-plate interactions, are included in this calculation and the long-range contributions of the Coulomb forces are taken into account via integration over infinitely many periodically repeated cells. If the movement of a charge reduces the energy of the system, the new state is unconditionally accepted, while otherwise the movement is allowed only with a certain probability that depends exponentially on the energy difference.

Finally, the surface-charge density γ and the dipole-moment density ζ are calculated from the integrals in (3), where the charge concentration χ is the result of the MMC simulation.

3.2.2 The Poisson-Boltzmann equation

The most-common and well-established continuum model for the description of ionic concentrations and the electrostatic interactions is the Poisson-Boltzmann equation (Lu et al., 2008). It is one of the most important equations in computational chemistry and often used to calculate ionic concentrations around molecules and the applications considered here, also at surfaces (Talasaz et al., 2006). The domain Ω is partitioned into two parts: the subdomain Ω_m of the molecule and the subdomain Ω_s of the solvent. Both regions are modeled by the nonlinear Poisson-Boltzmann equation

$$-\nabla \cdot (\varepsilon \nabla u) - \sum_{j=1}^{K} c_j q_j \mathrm{e}^{-\beta q_j u} = \sum_{i=1}^{N} p_i \delta(x - x_i) \quad \text{in } \Omega_s, \qquad (11a)$$

$$-\nabla \cdot (\varepsilon \nabla u) \qquad\qquad = \sum_{i=1}^{N} p_i \delta(x - x_i) \quad \text{in } \Omega_m, \qquad (11b)$$

where ε is again the permittivity, c_j is the bulk concentration of free ion species j with charge q_j, p_i is a charge at x_i in Ω_m, and $\beta = 1/kT$, where k is the Boltzmann constant and T is the temperature.

On the interface between the two subdomains Ω_m and Ω_s, continuity equations for the potential u and the dielectric displacement (i.e., the permittivity times the normal derivative),

$$[u] = 0, \qquad (12)$$

$$\left[\varepsilon \frac{\partial u}{\partial n} \right] = 0, \qquad (13)$$

where [.] denotes the difference of the limits in Ω_m and in Ω_s analogously to equations (2).

A leading special case of the PBE is the PBE for a symmetric, $1 : 1$ electrolyte (Holst et al., 2012). With $K = 2$, the bulk concentration $c_j = c$, and $q_j = (-1)^j q$, equation (11a) simplifies to

$$-\nabla \cdot (\varepsilon \nabla u) + 2cq \sinh(\beta q u) = \sum_{i=1}^{N} p_i \delta(x - x_i). \qquad (14)$$

This equation can be solved by various numerical methods such as the finite-difference method, the finite-volume method, or the boundary-element method (Lu et al., 2008). Nowadays several PBE solvers such as DelPhi (Honig and Nicholls, 1995), GRASP (Nicholls et al., 1991), MEAD (Bashford

and Gerwert, 1992), UHBD (Davis et al., 1991), PBEQ (Im et al., 1998), APBS (Baker et al., 2000; Holst et al., 2000), and AFMPB (Lu et al., 2010a), are available for biochemistry and biophysics.

A stochastic version of the Poisson-Boltzmann equation was also used to quantify fluctuations in nanowire field-effect biosensors (Heitzinger et al., 2010a).

3.2.3 PROPKA

An empirical method for the calculation of protein charges and pK_a values is the FORTRAN program PROPKA (Li et al., 2005; Bas et al., 2008; Olsson et al., 2011; Rostkowski et al., 2011). This method uses the structure of proteins from PDB files to compare it with empirical data. An initial guess for the pK_a value pK_a^{water} of a titrable group in water is perturbated by the change $\Delta pK_a^{\text{water}\to\text{protein}}$ of the pK_a value due to the protein, i.e., the pK_a value is

$$pK_a = pK_a^{\text{water}} + \Delta pK_a^{\text{water}\to\text{protein}} \tag{15}$$

according to (Søndergaard et al., 2011). Here pK_a^{water} is obtained empirically and is well-known, while $\Delta pK_a^{\text{water}\to\text{protein}}$ is calculated by PROPKA.

From comparison with empirical data and investigations of the structure of the proteins in PDB files, the main contributions to $\Delta pK_a^{\text{water}\to\text{protein}}$ have been detected and approximated. In PROPKA 3.1, these contributions are

$$\Delta pK_a^{\text{water}\to\text{protein}} = \Delta pK_a^{\text{desolv}} + \Delta pK_a^{\text{HB}} + \Delta pK_a^{\text{RE}} + \Delta pK_a^{\text{QQ}}, \tag{16}$$

where $\Delta pK_a^{\text{desolv}}$ describes the desolvation effects, ΔpK_a^{HB} describes the hydrogen-bond interactions, ΔpK_a^{RE} describes the contribution due to electrostatic reorganization energies, and ΔpK_a^{QQ} describes the Coulombic interactions. The Coulomb contribution due to charge-charge interactions is described for the protein residue i and a charge j from a charged or ionizable group as

$$\Delta pK_{a,i}^{QQ} = \frac{244\sigma_{ij}}{\varepsilon r_{ij}} w^{QQ}(r_{ij}), \tag{17a}$$

$$w^{QQ}(r_{ij}) = \begin{cases} \frac{r_{ij}}{r_{min}} & \text{if } r_{ij} \leq r_{min}, \\ \frac{r_{ij}-r_{min}}{r_{max}-r_{min}} & \text{if } r_{min} \leq r_{ij} \leq r_{max}, \\ 0 & \text{if } r_{ij} \geq r_{max}, \end{cases} \tag{17b}$$

$$\sigma_{ij} = \begin{cases} -1 & \text{if } (i \in \text{acids and } j \in \text{bases}) \\ & \text{or } (i \in \text{bases and } pK_{a,i} < pK_{a,j}), \\ +1 & \text{if } (i \in \text{bases and } j \in \text{acids}) \\ & \text{or } (i \in \text{acids and } pK_{a,i} > pK_{a,j}), \\ 0 & \text{else,} \end{cases} \tag{17c}$$

where 244 is the Coulomb's-law coefficient in pK_a units, ε is the dielectric constant, and σ gives the direction of the pK_a shift. Furthermore r_{ij} is the distance between the charge centers and w is a weight function.

Short-distance contributions $\Delta pK_{a,i}^{HB}$ from hydrogen bonds or contributions $\Delta pK_{a,i}^{RE}$ from reversed hydrogen bonds are modeled as

$$\Delta pK_{a,i}^{HB} = \begin{cases} c^{HB} w^{HB}(r_{ij}) \cos\theta & \text{if } \theta \geq 90°, \\ 0 & \text{else,} \end{cases} \quad (18a)$$

$$w^{HB}(r_{ij}) = \begin{cases} 1 & \text{if } r_{ij} \leq r_{min}, \\ \frac{r_{ij} - r_{min}}{r_{max} - r_{min}} & \text{if } r_{min} \leq r_{ij} \leq r_{max}, \\ 0 & \text{if } r_{ij} \geq r_{max}, \end{cases} \quad (18b)$$

where c^{HB} is a fitted constant, w is a weight function, and θ is the angle between the hydrogen bond and the hydrogen acceptor. Furthermore r_{ij} is the hydrogen-bond distance.

The desolvation effect due to nearby, non-hydrogen atoms ($k = 1, \ldots, N$) with volume V_k is calculated as

$$\Delta pK_{a,i}^{desolv} = c \sum_{k=1}^{N} \frac{V_k}{r_{ik}^4}, \quad (19)$$

where c is an empirically determined constant and where the center of the atom k is a distance r_{ik} away from the center of residue i.

The charge of the molecule is the sum of the charges of the single amino acids $\sum q_i$. The charge q_i of the amino acid i can be calculated as (De Vico et al., 2010)

$$q_i = \frac{10^{pK_{a,i} - pH}}{1 + 10^{pK_{a,i} - pH}}. \quad (20)$$

3.3 Summary

In summary, many approaches for the simulation of the partial charges of molecules, and in particular of DNA and proteins, have been developed. The main advantage of empirical models is the very fast prediction of pK_a values and charges with simulation times in the seconds range. Since these methods contain parameters that have been fitted to a sample data set, they are expected to work reliably only for molecules similar to the sample set. Hence more physically motivated methods are desirable, but come at a computational cost. In any case, empirical methods provide good approximations for many proteins and other biomolecules.

The simulation of DNA is facilitated by their, in comparison, simple and periodic structure. The structure of the biomolecules also plays a crucial role for the pK_a value and the partial charge, e.g., proteins have different charges

	Physically motivated	Computational cost
Monte-Carlo methods	$++$	$-$
Continuum models	$+$	$+$
Empirical models	$-$	$++$

Table 1: Comparison of the main approaches to the simulation of boundary layers in field-effect sensors.

if they are folded or unfolded. Hence it is often not possible to model and simulate the charging state of molecules accurately within feasible time or with feasible computational resources.

All methods have their specific advantages and none is better than the rest regarding all criteria (see Table 1). Hence this area continues to be one of active research and it is highly relevant for the quantitative understanding of affinity based sensors.

Using the methods summarized here, the charge concentration in boundary layers as they occur in nanowire field-effect sensors can be simulated. Furthermore, a transport model for the charges in the semiconducting nanowire is needed in order to simulate the whole sensor system. This is discussed in the next section.

4   The current through the nanowire transducer

A realistic model for the charge transport through the nanowire transducer must be three-dimensional because of the real-world boundary conditions, namely the location of the source, drain, and backgate contacts (Stern et al., 2007a; Nair and Alam, 2007; Elfström et al., 2007; Elfström and Linnros, 2008).

In this section, we present a continuum model for charge transport through nanowires. Various models for particle transport in semiconductors have been developed focusing on different aspects; the two main approaches are the Boltzmann equation, equations derived thereof such as the drift-diffusion equations and diffusion-type equations (Heitzinger and Ringhofer, 2011), and Monte-Carlo methods. For the purposes of the simulation of field-effect sensors, continuum models are well-suited. The important aspect in field-effect sensors are the boundary layer and minute changes therein, and not so much advanced effects of charge transport in nanoscale structures.

In this simulation step, the boundary layer (the microscopic part of the model) and charge transport (the macroscopic part of the model) are joined in a self-consistent manner.

4.1   The drift-diffusion-Poisson system

The electric potential V is the solution of the Poisson equation

$$- \nabla \cdot (\varepsilon(x) \nabla V(x)) = \rho(x) \tag{21}$$

for the electric potential V, where $\rho(x)$ is the charge concentration and $x \in \Omega \subset \mathbb{R}^3$. When modeling semiconducting materials, the charge concentration includes the charge carriers, i.e., the electron concentration n and the hole concentration p. Furthermore, the doping concentration C_{dop} of the semiconductor is also part of the charge concentration. Hence we have the charge concentration for semiconductors defined as

$$\rho_{\mathrm{semi}}(x) := q(p(x) - n(x) + C_{\mathrm{dop}}(x)), \tag{22}$$

where q is the elementary charge.

The concentrations n and p of the charge carriers are the solutions of the drift-diffusion equations

$$\nabla \cdot J_n = R, \tag{23a}$$
$$\nabla \cdot J_p = -R, \tag{23b}$$
$$J_n = D_n \nabla n - \mu_n n \nabla V, \tag{23c}$$
$$J_p = -D_p \nabla p - \mu_p p \nabla V, \tag{23d}$$

where D_n and D_p are the electron and hole diffusion coefficients, μ_n and μ_p are their mobilities, J_n and J_p are their current densities, and R denotes the recombination rate (Markowich et al., 1990; Selberherr, 1984). An important model for the recombination rate is the Shockley-Read-Hall recombination rate

$$R_{\mathrm{SRH}} := \frac{np - n_i^2}{\tau_p(n + n_i) + \tau_n(p + n_i)}, \tag{24}$$

where n_i denotes the intrinsic charge concentration and τ_n and τ_p are the relaxation times of the electrons and holes, respectively. Furthermore, we assume that the Einstein relations $D_n = U_T \mu_n$ and $D_p = U_T \mu_p$ hold, where U_T is the thermal voltage.

4.2   Self-consistent simulations of sensor systems

We have now all parts for a self-consistent model of NWFETs. We consider the typical structure of a nanowire sensor as depicted on the left-hand side of Fig. 3. The nanowire is covered by a thin, dielectric layer of oxide and surrounded by the aqueous solution containing the target molecules. Hence the simulation domain Ω can be partitioned into three subdomains Ω_{Si}, Ω_{ox}, and Ω_{liq} corresponding to these three materials. At the interface Γ between

(a) Device structure.   (b) Surface layer.
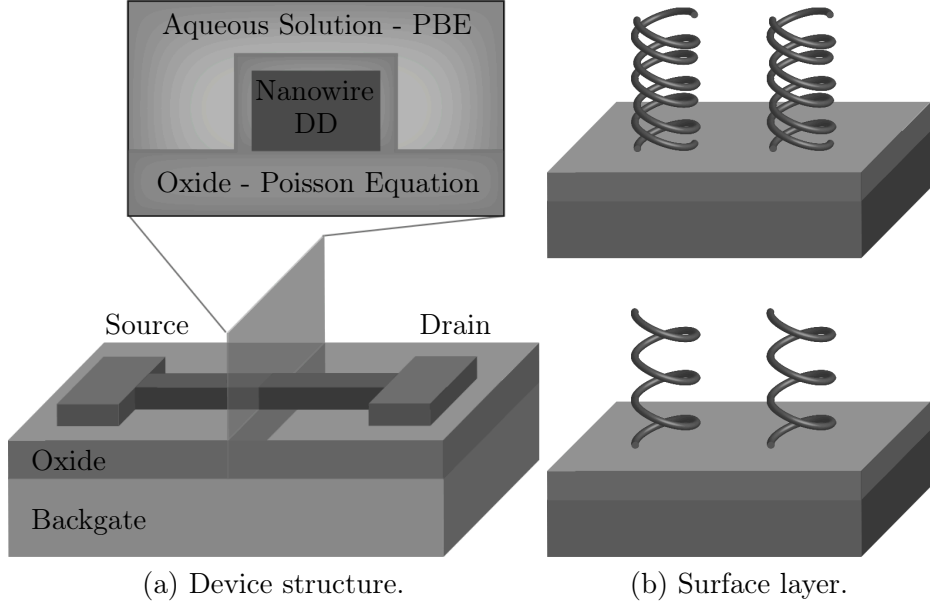
Figure 3: (a) Schematic diagram of the nanowire sensor; the different equations used in the simulation are indicated. (b) A nanowire functionalized with ssDNA as probes without any target molecules (bottom) and a nanowire functionalized with ssDNA with a target ssDNA strand (dsDNA, top).

the nanowire surface and the liquid, the charge concentration exhibits a fast varying spatial structure which leads to the multiscale problem discussed in Section 2. To simplify notation, the x-axis is always normal to the smooth interface Γ located at $x = 0$.

The equation for the potential is now the homogenized Poisson equation

$$-\nabla \cdot (\varepsilon(x,y,z)\nabla V(x,y,z)) = \begin{cases} \rho(x,y,z) & \text{in } \Omega_{\text{Si}} \cup \Omega_{\text{ox}}, \\ 0 & \text{in } \Omega_{\text{liq}}, \end{cases} \quad (25a)$$

$$V(0+,y,z) - V(0-,y,z) = \frac{\zeta(y,z)}{\varepsilon(0+)} \qquad \text{on } \Gamma, \quad (25b)$$

$$\varepsilon_{\text{liq}}\partial_x V(0+,y,z) - \varepsilon_{\text{ox}}\partial_x V(0-,y,z) = -\gamma(y,z) \qquad \text{on } \Gamma, \quad (25c)$$

where $0+$ denotes the limit at the interface in the outside of the nanowire, while $0-$ is the limit in the inside. The cumulative effect of the fast varying charge concentration in the surface layer is now given by the macroscopic dipole-moment density ζ and the macroscopic surface-charge density γ known from (3); they are calculated by the models in Section 3.

After modeling the charges in the boundary layer, we now turn to the charge concentration ρ in the remaining materials. In the semiconductor,

16

i.e., in Ω_{Si}, the Poisson equation is

$$-\nabla \cdot (\varepsilon_{\mathrm{Si}} \nabla V) = \rho_{\mathrm{semi}}(n, p), \qquad (26)$$

where $\rho_{\mathrm{semi}}(n, p)$ is given by the drift-diffusion equations in Section 4.1.

The aqueous solution Ω_{liq} is described by the Poisson-Boltzmann equation already discussed in Section 3.2.2. The charge concentration on the right-hand side is a hyperbolic sine (in the case of 1:1 electrolyte) with the bulk ionic concentration as a factor.

At the source, drain, and backgate contacts, Dirichlet boundary conditions hold, as well as at the electrode in the liquid if there is one (Lu et al., 2010b). Zero Neumann boundary conditions, i.e., vanishing electric fields, are used everywhere else. The inclusion of backgate contacts is crucial, since the operating regime of the sensor can be adjusted and optimized in this way (Baumgartner et al., 2011a,b).

The values of ζ and γ can be stored in look-up tables depending on the surface potential. Then the whole sensor can be simulated self-consistently using an enhanced Scharfetter-Gummel iteration scheme so that no computational penalty is paid compared to solving the classical drift-diffusion-Poisson system (Baumgartner and Heitzinger, 2012).

5 Summary

Nanowire sensors have been demonstrated experimentally in recent years and they are a technology that is currently being developed. Nanowire are extremely well-suited for sensing purposes due to their single-crystalline structure and their high surface-to-volume ratio.

Quantitative understanding of this new technology is crucial for the rational design and the optimization of various devices. The quantitative simulation of field-effect biosensors based on nanowires poses new challenges and the state-of-the-art of sensor simulation in this area is summarized here. Since this field has been receiving more and more attention, more work is certainly forthcoming.

The boundary layer containing the biomolecules at the nanowire transducer is responsible for sensitivity and selectivity. Therefore the boundary layer and its effect on the transducer are the crucial aspects of these field-effect sensors. Regarding modeling and simulation, these two aspects are novel compared to the well studied area of semiconductor devices and new intriguing questions arise. Hence the modeling and simulation of field-effect sensors goes beyond the modeling and simulation of semiconductor transistors.

The boundary layer must be modeled as realistically as possible. A mathematical method to achieve this in face of the multiscale aspect of the problem is to homogenize the partial differential equations that model the system. This allows us to simulate large structure while including effects on

the microscopic length scale, i.e., the length scale of single molecules in the boundary layer.

The screening of the partial charges of the biomolecules in the boundary layer can be simulated by continuum models such as the Poisson–Boltzmann equation and by atomistic models such as Metropolis-Monte-Carlo algorithms while calculating the partial charges by a model such as PROPKA.

Using self-consistent models, all relevant physical and geometrical properties can be included in the simulations. This makes it possible to provide realistic simulations and to predict sensitivity.

Acknowledgment

References

Alexov E., Mehler E., Baker N., Baptista A., Huang Y., Milletti F., Nielsen J., Farrell D., Carstensen T., Olsson M., Shen J., Warwicker J., Williams S., and Word J. (2011) Progress in the prediction of pKa values in proteins. *Proteins Struct. Funct. Bioinf.* **97**(12), 3260–3275. `http://dx.doi.org/10.1002/prot.23189`

Allen M. and Tildesley D. (1987) *Computer Simulation of Liquids.* Oxford University Press, Oxford, New York.

Baker N., Holst M., and Wang F. (2000) Adaptive multilevel finite element solution of the Poisson–Boltzmann equation II: Refinement at solvent accessible surfaces in biomolecular systems. *J. Comput. Chem.* **21**(15), 1343–1352. `http://dx.doi.org/10.1002/1096-987X(20001130) 21:15<1343::AID-JCC2>3.0.CO;2-K`

Bas D., Rogers D., and Jensen J. (2008) Very fast prediction and rationalization of pKa values for protein–ligand complexes. *Proteins Struct. Funct. Bioinf.* **73**(3), 765–783. `http://dx.doi.org/10.1002/prot.22102`

Bashford D. and Gerwert K. (1992) Electrostatic calculations of the pKa values of ionizable groups in bacteriorhodopsin. *J. Mol. Biol.* **224**(2), 473–486. `http://dx.doi.org/10.1016/0022-2836(92)91009-E`

Baumgartner S. and Heitzinger C. (2012) Existence and local uniqueness for 3d self-consistent multiscale models of field-effect sensors. *Commun. Math. Sci.* **10**(2), 693–716.

Baumgartner S., Vasicek M., Bulyha A., and Heitzinger C. (2011a) Optimization of nanowire DNA sensor sensitivity using self-consistent simulation. *Nanotechnology* **22**(42), 425503/1–8. `http://dx.doi.org/10.1088/0957-4484/22/42/425503`

Baumgartner S., Vasicek M., and Heitzinger C. (2011b) Analysis of field-effect biosensors using self-consistent 3D drift-diffusion and Monte-Carlo simulations. In *Proceedings of European Conference Eurosensors XXV 2011, September 4–7*, pages 1275/1–4, Athens, Greece.

Bergveld P. (1970) Development of an ion-sensitive solid-state device for neurophysiological measurements. *IEEE Trans. Biomed. Eng.* **17**(2), 70–71. `http://dx.doi.org/10.1109/TBME.1970.4502688`

Bergveld P. and Sibbald A. (1988) *Analytical and biomedical applications of ion-selective field-effect transistors*. Elsevier Amsterdam.

Bousse L., De Rooij N., and Bergveld P. (1983) Operation of chemically sensitive field-effect sensors as a function of the insulator-electrolyte interface. *IEEE Trans. Electron Devices* **30**(10), 1263–1270. `http://dx.doi.org/10.1109/T-ED.1983.21284`

Bulyha A. and Heitzinger C. (2011) An algorithm for three–dimensional Monte–Carlo simulation of charge distribution at biofunctionalized surfaces. *Nanoscale* **3**(4), 1608–1617. `http://dx.doi.org/10.1039/c0nr00791a`

Chen R., Bangsaruntip S., Drouvalakis K., Wong Shi Kam N., Shim M., Li Y., Kim W., Utz P., and Dai H. (2003) Noncovalent functionalization of carbon nanotubes for highly specific electronic biosensors. *PNAS* **100**(9), 4984–4989. `http://dx.doi.org/10.1073/pnas.0837064100`

Chen R., Choi H., Bangsaruntip S., Yenilmez E., Tang X., Wang Q., Chang Y., and Dai H. (2004) An investigation of the mechanisms of electronic sensing of protein adsorption on carbon nanotube devices. *JACS* **126**(5), 1563–1568. `http://dx.doi.org/10.1021/ja038702m`

Clark L. and Lyons C. (1962) Electrode systems for continuous monitoring in cardiovascular surgery. *Ann. N.Y. Acad. Sci.* **102**(1), 29–45. `http://dx.doi.org/10.1111/j.1749-6632.1962.tb13623.x`

Cui Y., Duan X., Hu J., and Lieber C. (2000) Doping and electrical transport in silicon nanowires. *J. Phys. Chem. B* **104**(22), 5213–5216. `http://dx.doi.org/10.1021/jp0009305`

Cui Y., Wei Q., Park H., and Lieber C. (2001) Nanowire nanosensors for highly sensitive and selective detection of biological and chemical species. *Science* **293**(5533), 1289–1292. `http://dx.doi.org/10.1126/science.1062711`

Cui Y., Zhong Z., Wang D., Wang W., and Lieber C. (2003) High performance silicon nanowire field effect transistors. *Nano Lett.* **3**(2), 149–152. `http://dx.doi.org/10.1021/nl025875l`

Davis M., Madura J., Luty B., and McCammon J. (1991) Electrostatics and diffusion of molecules in solution: simulations with the University of Houston Brownian dynamics program. *Comput. Phys. Commun.* **62**(2-3), 187–197. `http://dx.doi.org/10.1016/0010-4655(91)90094-2`

De Vico L., Iversen L., Sørensen M., Brandbyge M., Nygård J., Martinez K., and Jensen J. (2011) Predicting and rationalizing the effect of surface charge distribution and orientation on nano-wire based FET bio-sensors. *Nanoscale* **3**(9), 3635–3640. `http://dx.doi.org/10.1039/c1nr10316d`

De Vico L., Sørensen M., Iversen L., Rogers D., Sørensen B., Brandbyge M., Nygård J., Martinez K., and Jensen J. (2010) Quantifying signal changes in nano-wire based biosensors. *Nanoscale* **3**(2), 706–717. `http://dx.doi.org/10.1039/c0nr00442a`

Elfström N., Juhasz R., Sychugov I., Engfeldt T., Karlström A., and Linnros J. (2007) Surface charge sensitivity of silicon nanowires: Size dependence. *Nano Lett.* **7**(9), 2608–2612. `http://dx.doi.org/10.1021/nl0709017`

Elfström N., Karlström A., and Linnros J. (2008) Silicon nanoribbons for electrical detection of biomolecules. *Nano Lett.* **8**(3), 945–949. `http://dx.doi.org/10.1021/nl080094r`

Elfström N. and Linnros J. (2008) Biomolecule detection using a silicon nanoribbon: accumulation mode versus inversion mode. *Nanotechnology* **19**(23), 235201/1–5. `http://dx.doi.org/10.1088/0957-4484/19/23/235201`

Gao X., Zheng G., and Lieber C. (2010) Subthreshold regime has the optimal sensitivity for nanowire FET biosensors. *Nano Lett.* **10**(2), 547–552. `http://dx.doi.org/10.1021/nl9034219`

Hahm J. and Lieber C. (2004) Direct ultrasensitive electrical detection of DNA and DNA sequence variations using nanowire nanosensors. *Nano Lett.* **4**(1), 51–54. `http://dx.doi.org/10.1021/nl034853b`

Harame D., Bousse L., Shott J., and Meindl J. (1987) Ion-sensing devices with silicon nitride and borosilicate glass insulators. *IEEE Trans.*

Electron Devices **34**(8), 1700–1707. http://dx.doi.org/10.1109/T-ED.1987.23140

Heitzinger C., Liu Y., Mauser N.J., Ringhofer C., and Dutton R.W. (2010a) Calculation of fluctuations in boundary layers of nanowire field-effect biosensors. *J. Comput. Theor. Nanosci.* **7**(12), 2574–2580, doi: 10.1166/jctn.2010.1644. http://dx.doi.org/10.1166/jctn.2010.1644

Heitzinger C., Mauser N., and Ringhofer C. (2010b) Multiscale modeling of planar and nanowire field-effect biosensors. *SIAM J. Appl. Math.* **70**(5), 1634–1654. http://dx.doi.org/10.1137/080725027

Heitzinger C. and Ringhofer C. (2011) A transport equation for confined structures derived from the Boltzmann equation. *Commun. Math. Sci.* **9**(3), 829–857.

Holst M., Baker N., and Wang F. (2000) Adaptive multilevel finite element solution of the Poisson–Boltzmann equation I: Algorithms and examples. *J. Comput. Chem.* **21**(15), 1319–1342. http://dx.doi.org/10.1002/1096-987X(20001130)21:15<1319::AID-JCC1>3.0.CO;2-8

Holst M., McCammon J., Yu Z., Zhou Y., and Zhu Y. (2012) Adaptive finite element modeling techniques for the Poisson-Boltzmann equation. *Commun. Comput. Phys.* **11**(1), 179–214.

Honig B. and Nicholls A. (1995) Classical electrostatics in biology and chemistry. *Science* **268**(5214), 1144–1149. http://dx.doi.org/10.1126/science.7761829

Im W., Beglov D., and Roux B. (1998) Continuum solvation model: computation of electrostatic forces from numerical solutions to the Poisson-Boltzmann equation. *Comput. Phys. Commun.* **111**(1-3), 59–75. http://dx.doi.org/10.1016/S0010-4655(98)00016-2

Janata J. (2004) Thirty years of CHEMFETs–a personal view. *Electroanal.* **16**(22), 1831–1835. http://dx.doi.org/10.1002/elan.200403070

Kiyohara K. and Asaka K. (2007) Monte Carlo simulation of electrolytes in the constant voltage ensemble. *J. Chem. Phys.* **126**(21), 214704/1–14. http://dx.doi.org/10.1063/1.2736371

Kukic P. and Nielsen J. (2010) Electrostatics in proteins and protein–ligand complexes. *Future Med. Chem.* **2**(4), 647–666.

Li H., Robertson A., and Jensen J. (2005) Very fast empirical prediction and rationalization of protein pKa values. *Proteins Struct. Funct. Bioinf.* **61**(4), 704–721. http://dx.doi.org/10.1002/prot.20660

Li Y., Qian F., Xiang J., and Lieber C. (2006) Nanowire electronic and optoelectronic devices. *Mater. Today* **9**(10), 18–27. http://dx.doi.org/10.1016/S1369-7021(06)71650-9

Lu B., Cheng X., Huang J., and McCammon J. (2010a) AFMPB: an adaptive fast multipole Poisson–Boltzmann solver for calculating electrostatics in biomolecular systems. *Comput. Phys. Commun.* **181**(6), 1150–1160. http://dx.doi.org/10.1016/j.cpc.2010.02.015

Lu B., Zhou Y., Holst M., and McCammon J. (2008) Recent progress in numerical methods for the Poisson–Boltzmann equation in biophysical applications. *Commun. Comput. Phys.* **3**(5), 973–1009.

Lu M., Hsiao C., Lai W., and Yang Y. (2010b) Probing the sensitivity of nanowire-based biosensors using liquid-gating. *Nanotechnology* **21**(42), 425505/1–5. http://dx.doi.org/10.1088/0957-4484/21/42/425505

Markowich P., Ringhofer C., and Schmeiser C. (1990) *Semiconductor Equations.* Springer-Verlag New York, Inc. New York, NY, USA.

Nair P. and Alam M. (2007) Design considerations of silicon nanowire biosensors. *IEEE Trans. Electron Devices* **54**(12), 3400–3408. http://dx.doi.org/10.1109/TED.2007.909059

Nicholls A., Sharp K., and Honig B. (1991) Protein folding and association: insights from the interfacial and thermodynamic properties of hydrocarbons. *Proteins Struct. Funct. Bioinf.* **11**(4), 281–296. http://dx.doi.org/10.1002/prot.340110407

Olsson M., Søndergaard C., Rostkowski M., and Jensen J. (2011) PROPKA3: consistent treatment of internal and surface residues in empirical pKa predictions. *J. Chem. Theory Comput.* **7**(2), 525–537. http://dx.doi.org/10.1021/ct100578z

Patolsky F. and Lieber C. (2005) Nanowire nanosensors. *Mater. Today* **8**(4), 20–28. http://dx.doi.org/10.1016/S1369-7021(05)00791-1

Patolsky F., Timko B., Zheng G., and Lieber C. (2007) Nanowire-based nanoelectronic devices in the life sciences. *MRS Bull.* **32**(2), 142–149. http://dx.doi.org/10.1557/mrs2007.47

Patolsky F., Zheng G., and Lieber C. (2006a) Fabrication of silicon nanowire devices for ultrasensitive, label-free, real-time detection of biological and chemical species. *Nat. Protoc.* **1**(4), 1711–1724. http://dx.doi.org/10.1038/nprot.2006.227

Patolsky F., Zheng G., and Lieber C. (2006b) Nanowire-based biosensors. *Anal. Chem.* **78**(13), 4260–4269. http://dx.doi.org/10.1021/ac069419j

Patolsky F., Zheng G., and Lieber C. (2006c) Nanowire sensors for medicine and the life sciences. *Nanomed.* **1**(1), 51–65. `http://dx.doi.org/10.2217/17435889.1.1.51`

Pavliotis G. and Stuart A. (2007) *Multiscale Methods: Averaging and Homogenization.* Springer-Verlag, Berlin.

Poghossian A., Abouzar M., Amberger F., Mayer D., Han Y., Ingebrandt S., Offenhäusser A., and Schöning M. (2007) Field-effect sensors with charged macromolecules: Characterisation by capacitance–voltage, constant-capacitance, impedance spectroscopy and atomic-force microscopy methods. *Biosens. Bioelectron.* **22**(9–10), 2100–2107. `http://dx.doi.org/10.1016/j.bios.2006.09.014`

Rostkowski M., Olsson M., Søndergaard C., and Jensen J. (2011) Graphical analysis of pH-dependent properties of proteins predicted using PROPKA. *BMC Struct. Biol.* **11**(6), 1–6.

Schöning M. and Poghossian A. (2002) Recent advances in biologically sensitive field-effect transistors (BioFETs). *Analyst* **127**(9), 1137–1151. `http://dx.doi.org/10.1039/b204444g`

Schöning M. and Poghossian A. (2006) Bio FEDs (field-effect devices): State-of-the-art and new directions. *Electroanal.* **18**(19–20), 1893–1900. `http://dx.doi.org/10.1002/elan.200603609`

Selberherr S. (1984) *Analysis and Simulation of Semiconductor Devices.* Springer Verlag Wien New york.

Søndergaard C., Olsson M., Rostkowski M., and Jensen J. (2011) Improved treatment of ligands and coupling effects in empirical calculation and rationalization of pKa values. *J. Chem. Theory Comput.* **7**(7), 2284–2295. `http://dx.doi.org/10.1021/ct200133y`

Sørensen M., Mortensen N., and Brandbyge M. (2007) Screening model for nanowire surface-charge sensors in liquid. *Appl. Phys. Lett.* **91**(10), 102105/1–3. `http://dx.doi.org/10.1063/1.2779930`

Stern E., Klemic J., Routenberg D., Wyrembak P., Turner-Evans D., Hamilton A., LaVan D., Fahmy T., and Reed M. (2007a) Label-free immunodetection with CMOS-compatible semiconducting nanowires. *Nature* **445**(7127), 519–522. `http://dx.doi.org/10.1038/nature05498`

Stern E., Steenblock E., Reed M., and Fahmy T. (2008) Label-free electronic detection of the antigen-specific T-cell immune response. *Nano Lett.* **8**(10), 3310–3314. `http://dx.doi.org/10.1021/nl801693k`

Stern E., Vacic A., Rajan N., Criscione J., Park J., Ilic B., Mooney D., Reed M., and Fahmy T. (2010) Label-free biomarker detection from whole blood. *Nat. Nanotechnol.* **5**(2), 138–142. `http://dx.doi.org/10.1038/nnano.2009.353`

Stern E., Wagner R., Sigworth F., Breaker R., Fahmy T., and Reed M. (2007b) Importance of the Debye screening length on nanowire field effect transistor sensors. *Nano Lett.* **7**(11), 3405–3409, doi:10.1021/nl071792z. `http://dx.doi.org/10.1021/nl071792z`

Talasaz A.H., Nemat-Gorgani M., Liu Y., Ståhl P., Dutton R.W., Ronaghi M., and Davis R.W. (2006) Prediction of protein orientation upon immobilization on biological and nonbiological surfaces. *Proc. Nat. Acad. Sci. U.S.A.* **103**(40), 14773–14778.

Tian B., Cohen-Karni T., Qing Q., Duan X., Xie P., and Lieber C. (2010) Three-dimensional, flexible nanoscale field-effect transistors as localized bioprobes. *Science* **329**(5993), 830–834. `http://dx.doi.org/10.1126/science.1192033`

Timko B., Cohen-Karni T., Qing Q., Tian B., and Lieber C. (2010) Design and implementation of functional nanoelectronic interfaces with biomolecules, cells, and tissue using nanowire device arrays. *IEEE Trans. Nanotechnol.* **9**(3), 269–280. `http://dx.doi.org/10.1109/TNANO.2009.2031807`

Wang W., Chen C., Lin K., Fang Y., and Lieber C. (2005) Label-free detection of small-molecule–protein interactions by using nanowire nanosensors. *PNAS* **102**(9), 3208–3212. `http://dx.doi.org/10.1073/pnas.0406368102`

Xu J., Luo X., and Chen H. (2005) Analytical aspects of FET-based biosensors. *Front. Biosci.* **10**(1), 420–430. `http://dx.doi.org/10.2741/1538`

Zheng G., Gao X., and Lieber C. (2010) Frequency domain detection of biomolecules using silicon nanowire biosensors. *Nano Lett.* **10**(8), 3179–3183. `http://dx.doi.org/10.1021/nl1020975`

Zheng G., Patolsky F., Cui Y., Wang W., and Lieber C. (2005) Multiplexed electrical detection of cancer markers with nanowire sensor arrays. *Nat. Biotechnol.* **23**(10), 1294–1301. `http://dx.doi.org/10.1038/nbt1138`